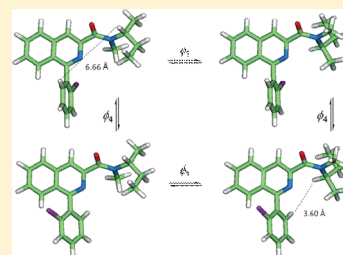


# Solution Structures of the Prototypical 18 kDa Translocator Protein Ligand, PK 11195, Elucidated with $^1\text{H}/^{13}\text{C}$ NMR Spectroscopy and Quantum Chemistry

Yong-Sok Lee,<sup>†</sup> Fabrice G. Siméon,<sup>‡</sup> Emmanuelle Briard,<sup>‡</sup> and Victor W. Pike\*<sup>†,‡</sup><sup>†</sup>Center for Molecular Modeling, Division of Computational Bioscience, Center for Information Technology, National Institutes of Health, Building 12a, Room 2049, Bethesda, Maryland 20892, United States<sup>‡</sup>PET Radiopharmaceutical Sciences Section, Molecular Imaging Branch, National Institute of Mental Health, National Institutes of Health, Building 10, Room B3 C346A, 10 Center Drive, Bethesda, Maryland 20892, United States

## S Supporting Information

**ABSTRACT:** Eighteen kilodalton translocator protein (TSPO) is an important target for drug discovery and for clinical molecular imaging of brain and peripheral inflammatory processes. PK 11195 [**1a**; 1-(2-chlorophenyl)-*N*-methyl-(1-methylpropyl)-3-isoquinoline carboxamide] is the major prototypical high-affinity ligand for TSPO. Elucidation of the solution structure of **1a** is of interest for understanding small-molecule ligand interactions with the lipophilic binding site of TSPO. Dynamic  $^1\text{H}/^{13}\text{C}$  NMR spectroscopy of **1a** revealed four quite stable but interconverting rotamers, due to amide bond and 2-chlorophenyl group rotation. These rotamers have been neglected in previous descriptions of the structure of **1a** and of the binding of **1a** to TSPO. Here, we used quantum chemistry at the level of B3LYP/6-311+G(2d,p) to calculate  $^{13}\text{C}$  and  $^1\text{H}$  chemical shifts for the rotamers of **1a** and for the very weak TSPO ligand, *N*-desmethyl-PK 11195 (**1b**). These data, plus experimental NMR data, were then used to characterize the structures of rotamers of **1a** and **1b** in organic solution. Energy barriers for both the amide bond and 2'-chlorophenyl group rotation of **1a** were determined from dynamic  $^1\text{H}$  NMR to be similar (ca. 17 to 18 kcal/mol), and they compared well with those calculated at the level of B3LYP/6-31G\*. Furthermore, the computed barrier for *Z* to *E* rotation is considerably lower in **1a** (18.7 kcal/mol) than in **1b** (25.4 kcal/mol). NMR (NOE) unequivocally demonstrated that the *E* rotamer of **1a** is the more stable in solution by about 0.4 kcal/mol. These detailed structural findings will aid future TSPO ligand design and support the notion that TSPO prefers to bind ligands as amide *E*-rotamers.



**KEYWORDS:** PK 11195, dynamic  $^1\text{H}/^{13}\text{C}$  NMR, TSPO, rotamer, variable temperature, energetics, quantum chemistry, structure

PK 11195 (1-(2-chlorophenyl)-*N*-methyl-(1-methylpropyl)-3-isoquinoline carboxamide, **1a** (Chart 1),<sup>1</sup> is the major prototypical high-affinity ligand for the 18 kDa translocator protein (TSPO), formerly known as the peripheral benzodiazepine receptor. TSPO was first discovered as a result of its ability to bind diazepam<sup>2</sup> and was later distinguished from central benzodiazepine receptors by location, function, structure, and pharmacology.<sup>3–5</sup> Several functions have been postulated for TSPO but perhaps the most evidence-based is as a mitochondrial membrane-based transporter, channel, or exchanger for cholesterol.<sup>6</sup> Besides isoquinoline carboxamides<sup>7</sup> and certain benzodiazepines (e.g., **2**; Ro-5-4864, 4-chlorodiazepam; Chart 1), TSPO also binds with high affinity to ligands belonging to many other structural classes<sup>8,9</sup> including quinoline carboxamides,<sup>10</sup> pyrazolopyrimidine acetamides,<sup>11</sup> 2-arylindole-3-acetamides,<sup>12</sup> *N,N*-dialkyl-2-phenylindol-3-ylglyoxylamides,<sup>13</sup> and aryloxyanilides<sup>14–16</sup> (Chart 1). High-affinity ligands from these and other structural classes invariably feature a single tertiary amido group.<sup>8,9</sup>

TSPO is now implicated in various neuropsychiatric conditions, especially anxiety, and is expressed heavily in microglia in response to various inflammatory conditions in brain and

periphery.<sup>17,18</sup> TSPO has therefore become a significant target for CNS drug development.<sup>9</sup> Furthermore, radioligands<sup>19–21</sup> for the imaging of TSPO *in vivo* are keenly pursued as potential biomarkers of inflammatory conditions.<sup>22,23</sup> These considerations drive the efforts to discover new and selective high-affinity TSPO ligands as potential new CNS drugs or improved imaging radioligands.

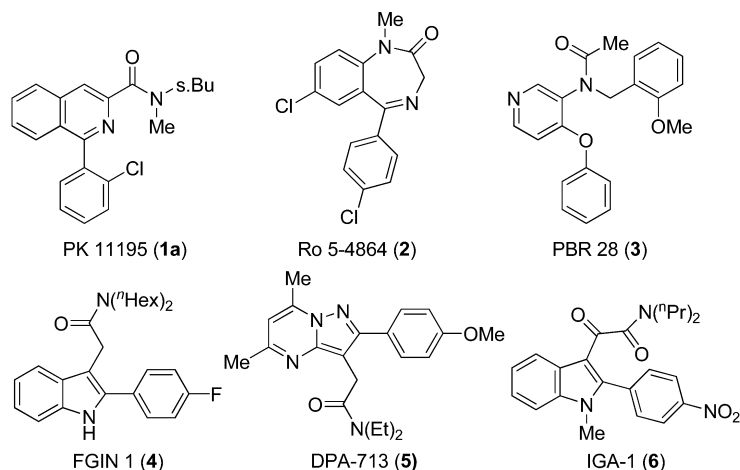
The interaction of **1a** and other ligands with TSPO has been modeled extensively.<sup>24–27</sup> From these studies, it is clear that the amido carbonyl group of **1a** plays a critical role in its binding to TSPO, perhaps by forming a directional hydrogen bond within a generally lipophilic binding site. Hence, precise knowledge of the position and orientation of the carbonyl group of **1a** in solution and when bound to TSPO can be informative about the topography of the TSPO binding site, and also aid in future ligand design. Earlier studies have not considered the possible existence of stable rotamers of **1a** in solution (Figure 1), nor

Received: January 20, 2012

Revised: February 8, 2012

Accepted: February 14, 2012

Published: February 14, 2012

Chart 1. Some High Affinity TSPO Ligands from Different Structural Classes<sup>a</sup>

<sup>a</sup>PK 11195 (1a; an isoquinoline carboxamide); Ro 5-4864 (2; a benzodiazepine); PBR 28 (3; an aryloxyanilide); FGIN 1 (4; an indoleacetamide); DPA-713 (5; a pyrazolopyrimidine); IGA-1 (6; an *N*<sup>1</sup>-methyl-2-phenylindol-3-ylglyoxylamide).

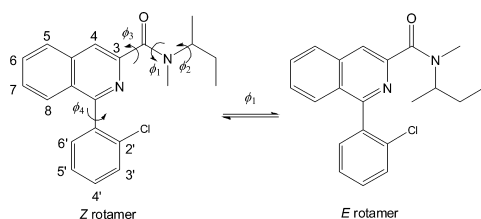


**Figure 1.** *Z/E* isomerization of **1a** through rotation of the dihedral angle of  $\text{CH}_3\text{-N-C=O}$  ( $\phi_1$ );  $\phi_2$ ,  $\phi_3$ , and  $\phi_4$  are the respective dihedral angles for  $\text{CH}_3\text{-CH-N-CO}$ ,  $\text{O=C-C3-C4}$ , and  $\text{C2'-C1'-C1-N}$ .

considered the possible roles of such rotamers in the binding of **1a** to TSPO. Here, we performed dynamic NMR spectroscopy and quantum chemical studies on **1a** that reveal four stable rotamers for **1a** in solution that are due to amide bond and chlorophenyl group rotation. Our findings lead us to suggest that TSPO prefers to bind amide ligands as *E* rotamers and will inform future TSPO ligand and radiotracer design.

## RESULTS AND DISCUSSION

**Characterization of the Isomers of 1a.** <sup>1</sup>H NMR spectroscopy (400 MHz) of **1a** in  $\text{CDCl}_3$  (Figure S1, Supporting Information) or *d*<sub>6</sub>-DMSO (Figure S2) at room temperature revealed the presence of amide bond rotamers. Signals for the *N*-methyl group protons in  $\text{CDCl}_3$  are well separated for each rotamer ( $\delta$  2.90 and 2.98), as are those for the *s*-butyl group protons (Table 1). The signals for the *s*-butyl  $\text{CH}_2$  and  $\text{CHCH}_3$  protons appear at lower field for the major rotamer than for the minor rotamer. However, signals for the *s*-butyl CH and  $\text{CH}_2\text{CH}_3$  protons in the rotamers are reversed, with that at higher field belonging to the major rotamer. This reversal may be attributed to the magnetic anisotropy of the carbonyl bond.<sup>28</sup> For each pair of signals arising from chemically equivalent protons, the ratio of the integral for the major rotamer to that of the minor rotamer is in the range 1.8–2.0, indicating that the major rotamer is more stable than the minor rotamer in organic solution by about 0.4 kcal/mol. In addition, the <sup>1</sup>H NMR (400 MHz) spectrum of **1a** in  $\text{CDCl}_3$  at room temperature (Figure S1, Supporting Information; Table 1) clearly revealed an interesting unexpected feature for the signals

of the *N*-methyl protons in the *E* and *Z* rotamers that was not seen in the spectra acquired in *d*<sub>6</sub>-DMSO (Figure S2, Supporting Information). Namely, each signal appeared not as the expected singlet but as an almost completely resolved pair of peaks with small separation (<0.015 ppm) and unequal height, with that at lower field showing lower intensity. We suspected the existence of these paired peaks as being due to 2-chlorophenyl group rotamers.

The <sup>13</sup>C NMR spectrum of **1a** in  $\text{CDCl}_3$  at 24 °C (Figure S3, Supporting Information) also showed pairs of prominent signals for each alkyl carbon that are well separated at upper field with an intensity ratio comparable to that seen for the <sup>1</sup>H signals. For example, the intensity of the doublet signal at  $\delta$  55.75 and 55.57 is about 2-fold higher than the one at  $\delta$  50.58 and 50.38, suggesting that this pair of doubled signals, with a separation of more than 5 ppm, arises from amide bond rotamers in solution. Furthermore, the fact that each signal appeared as a very narrow doublet (separation  $\leq$ 0.2 ppm), as seen in the signals of the *N*-methyl protons, again indicated that another pair of rotamers exists for each of the amide bond isomers.

While <sup>1</sup>H/<sup>13</sup>C COSY NMR experiments (Figure S4, Supporting Information) allowed correlation of the <sup>1</sup>H and <sup>13</sup>C signals (e.g., those for C and H in the CH group of the *s*-butyl group) in the same rotamer, they cannot identify the rotamers or their geometries. Accordingly, we resorted to quantum mechanical calculations, utilizing density functional theory (DFT) at the level of B3LYP/6-311+G(2d,p) in the reaction field of chloroform, to obtain the structures and energetics of **1a** rotamers as well as estimates of their <sup>1</sup>H and <sup>13</sup>C NMR chemical shifts.

Figure 2 shows four fully geometry-optimized isomers of **1a**, which we dub *Z*<sub>1</sub>, *Z*<sub>2</sub>, *E*<sub>1</sub>, and *E*<sub>2</sub>. The *Z*<sub>1</sub> isomer was modeled after the reported tetrameric X-ray structure of **1a** showing a highly disordered *s*-butyl region,<sup>29</sup> whereas *E*<sub>1</sub> was obtained by rotating the *N*-methyl group of the *Z*<sub>1</sub> rotamer with respect to the amide C–N bond. Both *Z*<sub>1</sub> and *E*<sub>1</sub> display an *exo* orientation of the carbonyl group to the isoquinolinyl ring and a near orthogonality between this ring and the chlorophenyl group. The optimized *Z*<sub>1</sub> structure closely resembles the X-ray structure of higher occupancy fragment with a heavy atom root-mean-square deviation (rmsd) of 0.36 Å. When omitting

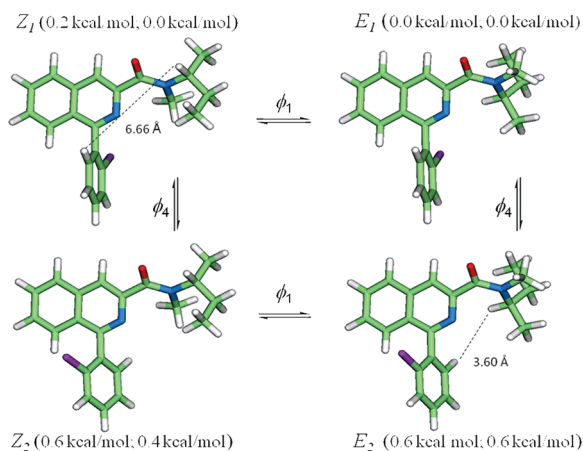


**Figure 2.** Geometry-optimized *Z* and *E* isomers of **1a** at the level of B3LYP/6-311+G(2d,p) in the solvent reaction field of chloroform. Values in parentheses represent the total electronic energy and the Gibbs free energy at 298.15 K, respectively, relative to those of the *E*<sub>1</sub> isomer. The amide bond isomerization, *Z*<sub>1</sub> to *E*<sub>1</sub> or *Z*<sub>2</sub> to *E*<sub>2</sub>, was done by varying  $\phi_1$  centered on the C–N bond; conversion of *Z*<sub>1</sub> into *Z*<sub>2</sub> or *E*<sub>1</sub> into *E*<sub>2</sub> was done by varying  $\phi_4$  centered on the C1–C1' bond. Dashed lines indicate the distances between the CH and C6H protons. Atoms are colored as follows: white, hydrogen; green, carbon; blue, nitrogen; red, oxygen; violet, chlorine.

consideration of the 2-chlorophenyl group, the rmsd decreased to 0.16 Å, showing that the rmsd of 0.36 Å is largely due to the difference in  $\phi_4$  [−102.9° (calculated) vs −78.2° (X-ray)]. The other calculated dihedral angles defined in Figure 1, [i.e.,  $\phi_1$  (−168.8°),  $\phi_2$  (−100.6°), and  $\phi_3$  (48.5°)] are more similar to those of the X-ray structure [ $\phi_1$  (−162.8°),  $\phi_2$  (−95.4°), and  $\phi_3$  (56.4°)]. The X-ray structure also depicts a conformer of *Z*<sub>1</sub> with dihedral angle,  $\phi_3 = -56.4^\circ$ . This conformer, having a counter-clockwise orientation of the amide plane relative to the isoquinoline ring of *Z*<sub>1</sub>, is discussed later in more detail.

When the chlorophenyl groups of *Z*<sub>1</sub> and *E*<sub>1</sub> were rotated with respect to their C1–C1' bonds by about 180°, calculations revealed another pair of stable rotamers, *Z*<sub>2</sub> and *E*<sub>2</sub>. In terms of the total electronic energy in the reaction field of chloroform, *E*<sub>1</sub> appears most stable among the four isomers. When the zero point correction and thermal free energy at 298.15 K were included, *Z*<sub>1</sub> and *E*<sub>1</sub> became isoenergetic and more stable than *Z*<sub>2</sub> and *E*<sub>2</sub> by 0.4 and 0.6 kcal/mol, respectively. The extra stability of both *Z*<sub>1</sub> and *E*<sub>1</sub> likely arises from lower steric repulsion between the amide oxygen pointing out of the plane and the C2'–Cl pointing into the plane (Figure 2). However, these calculated energy differences are too close to assign the observed more intense NMR peak of a pair to either the *Z*<sub>1</sub> or *E*<sub>1</sub> isomer. We therefore calculated NMR chemical shifts for each rotamer since such calculations are known to be very useful for assigning experimental <sup>1</sup>H and <sup>13</sup>C peaks to specific isomers.<sup>30</sup>

Figure 3 represents the four rotamers of **1a** with their calculated <sup>13</sup>C chemical shifts. For the rotamer identification, we selected four carbons (i.e., N-CH<sub>3</sub>, CHCH<sub>3</sub>, CHCH<sub>3</sub>, and C=O) in the amide region because the differential magnetic shieldings of these carbons are stronger than for others. For example, from the calculations, the N-CH<sub>3</sub> of *E*<sub>1</sub> ( $\delta$  29.20) *syn* to oxygen is much more strongly shielded than that of *Z*<sub>1</sub> ( $\delta$  32.97) *anti* to oxygen. Also, both CHCH<sub>3</sub> ( $\delta$  57.11) and CHCH<sub>3</sub> ( $\delta$  19.01) of *Z*<sub>1</sub> *syn* to oxygen are better shielded than the respective *anti* carbons of *E*<sub>1</sub> ( $\delta$  65.28,  $\delta$  20.34).

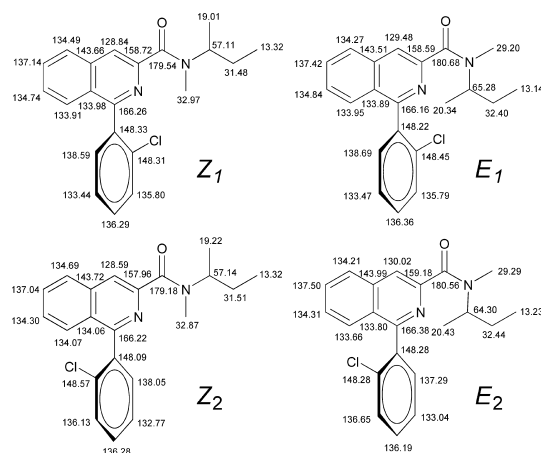


**Figure 3.** Calculated <sup>13</sup>C chemical shifts for four isomers of **1a** at the level of B3LYP/6-311+G(2d,p) in the solvent reaction field of chloroform.

The shielding and deshielding of the alkyl carbons of the *E* and *Z* isomers are consistent with previous <sup>13</sup>C NMR studies,<sup>31–34</sup> which have shown that alkyl carbon atoms *syn* to amide oxygen are better shielded than the corresponding *anti* carbons. In particular, the differential shielding of the *N*-methyl carbon was attributed either to the electric field caused by the carbonyl group<sup>33,34</sup> or to the paramagnetic contribution of the N–C bond of the *N*-methyl group.<sup>31</sup> Besides the *syn/anti* effect in upper field, our calculations further indicate that the carbonyl carbon in *Z*<sub>1</sub> ( $\delta$  179.54) is better shielded than in *E*<sub>1</sub> ( $\delta$  180.68), which can serve as a low field marker.

Whereas amide bond rotation results in sizable chemical shift differences between the alkyl carbons of *Z*<sub>1</sub> and *E*<sub>1</sub>, much smaller differences are seen for chlorophenyl group rotation between *Z*<sub>1</sub> and *Z*<sub>2</sub> or between *E*<sub>1</sub> and *E*<sub>2</sub> (Figure 3), in good agreement with the narrow doublet of each alkyl carbon signal observed experimentally (Figure S3, Supporting Information). For instance, the *s*-butyl CH of *Z*<sub>2</sub> ( $\delta$  57.14) is very slightly deshielded upon rotation of the chlorophenyl group of *Z*<sub>1</sub> ( $\delta$  57.11). Accordingly, the observed doublet at  $\delta$  50.38 and 50.58 can be assigned to the CH of *Z*<sub>1</sub> and *Z*<sub>2</sub>, respectively. Similarly, the doublets seen at  $\delta$  55.75 and 55.57 were assigned, respectively, to the calculated CH of *E*<sub>1</sub> ( $\delta$  65.28) and *E*<sub>2</sub> ( $\delta$  64.30). The upfield experimental <sup>13</sup>C peaks were assigned by using the calculated chemical shift caused by amide bond rotation as a major marker and those of the chlorophenyl group rotation for fine-tuning (Table S1, Supporting Information). Figure 4 depicts the experimental and calculated chemical shifts for the alkyl carbons of **1a** without the resolution of their chlorophenyl group rotamers. This assignment clearly demonstrates that (i) the *syn/anti* effect is stronger for CH and CH<sub>3</sub> directly bonded to the amide nitrogen and then gets progressively weaker for the more distal carbon atoms and (ii) that for any given pair, the experimental peak intensity assigned to *E* isomer is stronger.

Whereas use of calculated and experimental <sup>13</sup>C signals to identify *E* and *Z* isomers can be rather straightforward, use of <sup>1</sup>H signals is less certain due to the narrower span of chemical shifts. Moreover, for each methyl group the calculations provide three distinct signals, one for each methyl proton, whereas experimental <sup>1</sup>H NMR gives only a single signal at room temperature. This renders any comparison between theory and experiment more challenging. For **1a**, the *s*-butyl CH proton

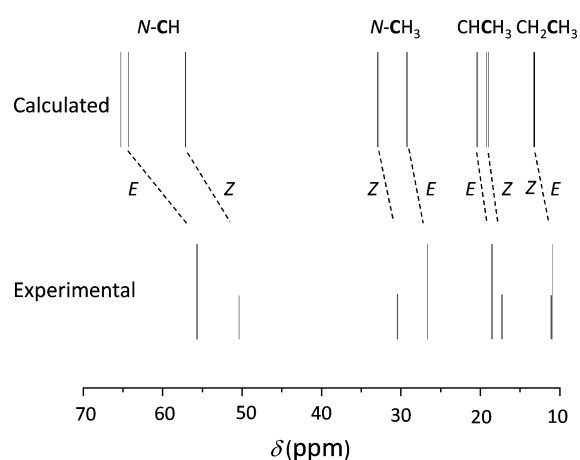


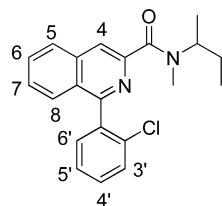
**Figure 4.** Pictorial comparison of the calculated and experimental  $^{13}\text{C}$  NMR spectra of *Z* and *E* of isomers of **1a** at upper field. Tall and short lines in the experimental spectrum indicate the respective major and minor signals, for each carbon.

turned out to be useful. The calculated chemical shifts indicate that the CH proton in  $E_1$  ( $\delta$  4.40) and  $E_2$  ( $\delta$  4.40) is better shielded than in  $Z_1$  ( $\delta$  5.32) and  $Z_2$  ( $\delta$  5.39), and this agrees well with the experiment (*E* rotamer,  $\delta$  3.89; *Z* rotamer,  $\delta$  4.80) based on relative peak intensity (Table 1). In general, protons *syn* to the amide oxygen are better shielded than those *anti*.<sup>35</sup> However, when a methine (CH) proton in the plane of the

amide group is conformationally restricted, such shielding is reversed.<sup>36</sup> The calculated energy barrier for the rotation of  $\phi_2$  of  $Z_1$  is about 11 kcal/mol, thereby confirming the constrained rotation of the *s*-butyl group with respect to the *N*-CH bond. The better experimental shielding of CHCH<sub>3</sub> protons in *Z* ( $\delta$  1.19) than in *E* ( $\delta$  1.22) and also of CH<sub>2</sub>CH<sub>3</sub> protons in *E* ( $\delta$  0.79) than in *Z* ( $\delta$  0.99) can be attributed to the *syn* effect to the amide oxygen as seen in Figure 2. Our experimental observation that the *N*-CH<sub>3</sub> is more strongly shielded in *Z* ( $\delta$  2.90) than in *E* ( $\delta$  2.98) is noteworthy in view of numerous reports that freely rotating *N*-methyl protons *syn* to an amide oxygen are better shielded.<sup>36,37</sup> In accord with experiment, calculation also shows the calculated *N*-CH<sub>3</sub> peaks are on average better shielded in  $Z_1$  ( $\delta$  2.90) than in  $E_1$  ( $\delta$  3.00). The geometry-optimized structures of **1a** (Figure 2) show that the *N*-CH<sub>3</sub> of  $Z_1$  but not of  $E_1$  is in the diamagnetic region of the isoquinolinyl ring current field and that this ring current likely causes the reversal of the *N*-CH<sub>3</sub> peaks.<sup>36,38</sup>

Both  $^1\text{H}$  and  $^{13}\text{C}$  peak intensity invariably favored assignment of *E* as the major rotamer of **1a** in solution. This does not fully agree with our calculations, which indicate that  $Z_1$  and  $E_1$  are isoenergetic. The only unambiguous experimental method for resonance assignment in tertiary amides is through observation of a clear nuclear Overhauser effect (NOE).<sup>39</sup> Accordingly, we searched for interactions between the *s*-butyl CH proton signal and those of the chlorophenyl group protons with NOE spectroscopy of **1a** in CDCl<sub>3</sub>. Only the major rotamer showed a

**Table 1.** Theoretical and Experimental  $^1\text{H}$ -NMR for **1a** in Chloroform



signal	chemical shift ( $\delta$ )			
	theory		experimental	
	$E_1$	$Z_1$	<i>E</i>	<i>Z</i>
CH <sub>2</sub> CH <sub>3</sub>	0.34	0.75	0.79	0.99
	0.77	0.89	(2 overlapping <i>t</i> , $J$ = 7.08 Hz)	(2 merging <i>t</i> , $J$ = 7.38 Hz)
	0.85	1.05		
CHCH <sub>3</sub>	0.78	1.02	1.22 ( <i>d</i> , $J$ = 6.55 Hz)	1.19 ( <i>d</i> , $J$ = 6.34 Hz)
	1.35	1.22		
	1.36	1.31	1.24 ( <i>d</i> , $J$ = 6.67 Hz)	
CH <sub>2</sub> CH <sub>3</sub>	1.37	1.62	1.66 ( <i>m</i> )	1.40 ( <i>m</i> )
	1.74	1.72		
	2.80	2.78	2.98 ( <i>d</i> )	2.90 ( <i>d</i> )
NCH <sub>3</sub>	2.82	2.85		
	3.38	3.08		
	4.40 (4.40) <sup>a</sup>	5.32 (5.39) <sup>a</sup>	3.89 ( <i>m</i> )	4.80 ( <i>m</i> )
ArH <sup>6'</sup>	7.93 (7.87) <sup>a</sup>	7.85 (7.95) <sup>a</sup>	7.66 ( <i>m</i> )	
ArH <sup>3'</sup>	8.13 (8.13) <sup>a</sup>	8.09 (8.16) <sup>a</sup>	7.37 ( <i>m</i> )	
ArH <sup>8</sup>	8.12 (8.0) <sup>a</sup>	8.10 (8.06) <sup>a</sup>	7.40 ( <i>m</i> )	
ArH <sup>5'</sup>	7.87 (7.83) <sup>a</sup>	7.90 (7.84) <sup>a</sup>	7.57 ( <i>m</i> )	
ArH <sup>4'</sup>	7.96 (7.85) <sup>a</sup>	7.96 (7.99) <sup>a</sup>	7.40 ( <i>m</i> )	
ArH <sup>7</sup>	8.15 (8.03) <sup>a</sup>	8.06 (8.08) <sup>a</sup>	7.57 ( <i>m</i> )	
ArH <sup>6</sup>	8.25 (8.23) <sup>a</sup>	8.21 (8.21) <sup>a</sup>	7.72 ( <i>m</i> )	
ArH <sup>5</sup>	8.56 (8.60) <sup>a</sup>	8.54 (8.55) <sup>a</sup>	7.96 ( <i>d</i> , $J$ = 8.33 Hz)	
ArH <sup>4</sup>	8.78 (8.87) <sup>a</sup>	8.74 (8.67) <sup>a</sup>	8.01 ( <i>d</i> )	8.05 ( <i>d</i> )

<sup>a</sup>Values in parentheses are for the respective  $E_2$  and  $Z_2$  isomers.



positive effect (Figure S5, Supporting Information), and therefore, we unambiguously assign this rotamer as *E* and the minor rotamer as *Z*. This result is consistent with the optimized structures of **1a** in Figure 2, which show that the *s*-butyl CH protons of *E*<sub>2</sub> and *Z*<sub>1</sub> are positioned at 3.60 Å and 6.66 Å away from their corresponding chlorophenyl group C6-H protons, respectively, whereas the *s*-butyl CH protons of *E*<sub>1</sub> and *Z*<sub>2</sub> are positioned at 5.32 Å and 6.91 Å away from their corresponding protons.

The preference for **1a** to exist as an *E* rotamer in organic solution contrasts with the existence of **1a** as a *Z* rotamer in the crystalline state.<sup>29</sup> Our calculations indicate that the *Z*<sub>1</sub> rotamer with the chlorine pointing into the plane (Figure 2) is more stable by 0.4 kcal/mol at room temperature than *Z*<sub>2</sub> with the chlorine pointing out of the plane. This finding agrees well with the X-ray structure that has shown 94% site-occupation for the chlorine at 2'-position corresponding to *Z*<sub>1</sub> in Figure 2. Nevertheless, it is puzzling why the *E* isomers become more stable by 0.4 kcal/mol than the *Z* isomers in organic solution. One plausible explanation is that the solvent reaction field, such as the polarizable continuum model (PCM) implemented in quantum chemistry software, may not fully account for the solvation of *Z* and *E* isomers by CHCl<sub>3</sub> or DMSO. Accurate estimation of the interaction energy between solute and solvent requires the explicit structure of the solvent, at least at the level of the first solvation shell.<sup>40</sup> Thus, while good at approximating the electrostatic interaction between solute and bulk solvent, the reaction field itself may not predict the solvent induced stability of the *E* over the *Z* isomer. In this case, the specific short-range solute–solvent interactions may be playing a critical role.

**Characterization of the Isomers of 1b.** In contrast to the findings on **1a**, both the <sup>1</sup>H (Figure S6, Supporting Information)- and <sup>13</sup>C NMR (Figure S7, Supporting Information) spectra of the corresponding *N*-desmethyl secondary amide **1b** at 24 °C in CDCl<sub>3</sub> showed no duplications of signals attributable to amide bond rotamers. The two possibilities are that the rotamers are rapidly interconverting on the NMR time-scale or that a single rotamer predominates.<sup>35</sup> Generally, most secondary amides are found to exist as *Z* rotamers only.<sup>35</sup> The calculated energetics of **1b** indicate that the geometry-optimized *Z* rotamer (Figure 5) is 5.8 kcal/mol

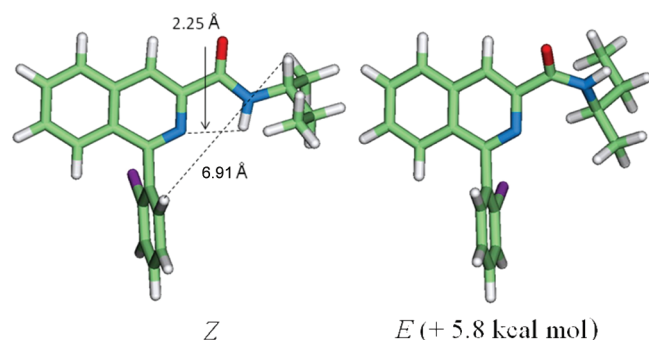


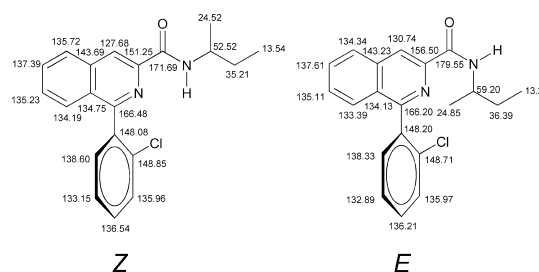
**Figure 5.** Geometry-optimized *Z* and *E* isomers of **1b**. Dashed lines indicate the distance between the hydrogens of CH and C6'H and also between the NH and the nitrogen of the isoquinoline ring. The value in parentheses represents the Gibbs free energy at 298.15 K with respect to that of the *Z* isomer.

more stable than the *E* rotamer, which implies that more than 99.99% of **1b** exists in *Z* form in organic solution at room temperature.

The large stability difference between the rotamers of **1b** arises from the spatial orientation of the amido hydrogen. In the *Z* rotamer, the isoquinolinyl nitrogen forms a hydrogen bond with the amide hydrogen. As a result, both the isoquinolinyl ring and the amide group are on the same plane ( $\phi_3 = 0.3^\circ$ ). By contrast, in the *E* rotamer, there is steric repulsion between the isoquinolinyl ring and the *s*-butyl group, resulting in a sizable distortion between the two planes ( $\phi_3 = 43.1^\circ$ ).

An NOE experiment revealed no interaction between the signal for the *s*-butyl CH proton and those of the protons in the chlorophenyl ring. This is consistent with the optimized geometry of *Z* (Figure 5) showing its *s*-butyl CH proton 6.70 Å away from the chlorophenyl group C6'H. The *s*-butyl CH proton of *E* can interact with the chlorophenyl group C6'H upon chlorophenyl group rotation. However, the NOE signal was not detected due to the thermochemical instability of the *E* rotamer. Hence, the *Z* configuration was assigned to **1b**. The <sup>1</sup>H NMR spectrum calculated for the *Z* rotamer of **1b** alone quite accurately predicts the key features of the experimental <sup>1</sup>H NMR spectrum (Table 2). Notably, the calculation suggests that the chemical shifts for the NH proton differ significantly between rotamers (*Z*,  $\delta$  8.74; *E*,  $\delta$  6.69), and this feature most distinguishes the spectra; the amide hydrogen in the *Z* isomer of **1b** *anti* to the oxygen is much more deshielded than in the *E* isomer. The signal for the NH proton in the experimental spectrum falls wholly between  $\delta$  8.04 and 8.06 and therefore, within the magnitude of computational error, is consistent with **1b** existing exclusively as the *Z* rotamer. As in the case of **1a**, the *s*-butyl CH proton of *E* ( $\delta = 4.36$ ) was calculated to be better shielded than that of *Z* ( $\delta$  4.98); experimentally, this proton was observed at  $\delta$  4.16.

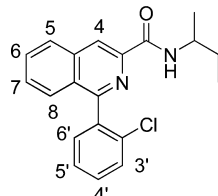
In line with the <sup>1</sup>H NMR study, the observed <sup>13</sup>C NMR spectrum of **1b** (Figure S7, Supporting Information) does not show a pair of amide isomers. As shown in Figure 6, the



**Figure 6.** Calculated <sup>13</sup>C chemical shifts for the *Z* and *E* isomers of **1b**.

calculated <sup>13</sup>C chemical shifts of the alkyl carbons, such as CHCH<sub>3</sub>, CHCH<sub>3</sub>, and CH<sub>2</sub>CH<sub>3</sub>, exhibit a pattern similar to that seen for **1a** in that the carbons *syn* to oxygen are better shielded than the corresponding *anti* carbons. For example, the *s*-butyl CH of *Z* ( $\delta$  52.52) *syn* to oxygen is 6.68 ppm better shielded than that of *E* ( $\delta$  59.20). Accordingly, the experimental chemical shift ( $\delta$  44.92) can be safely assigned to the CH of the *Z* isomer (Table S2, Supporting Information). Most of these alkyl carbon peaks also exist as a doublet separated by less than 0.07 ppm that can be attributed to chlorophenyl group rotation.

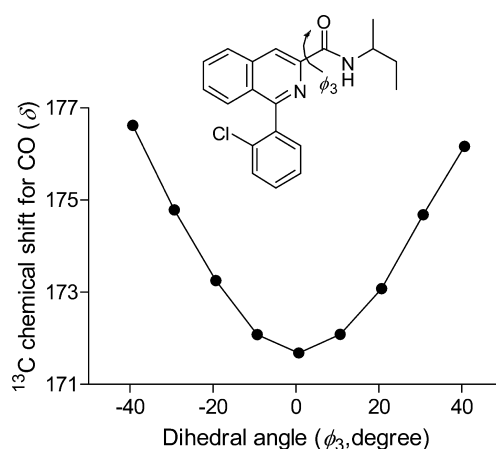
Besides the alkyl-carbons, our calculations suggest that the carbonyl carbon of *Z* in **1b** ( $\delta$  171.69) is unusually more strongly shielded than that of *E* ( $\delta$  179.55). Moreover, the chemical shift of the C=O of *desmethyl-E* is comparable to that of *Z*<sub>1</sub> ( $\delta$  179.54) and *E*<sub>1</sub> ( $\delta$  180.68) of **1a**. In line with the calculations, the experimental chemical shift for C=O in **1b**

**Table 2. Theoretical and Experimental  $^1\text{H}$  NMR Data for **1b** in Chloroform**


signal	chemical shift ( $\delta$ )		
	<i>E</i> (theory)	<i>Z</i> (theory)	experiment
$\text{CH}_2\text{CH}_3$	0.33	0.79	0.964 ( <i>t</i> , $J = 6.99$ Hz)
	0.87	0.93	
	1.05	1.05	
$\text{CHCH}_3$	0.95	0.95	1.27 ( <i>d</i> , $J = 6.62$ Hz)
	0.97	1.18	
	1.59	1.40	
$\text{CH}_2\text{CH}_3$	1.61	1.80	1.61 ( <i>m</i> )
	1.33	1.46	
CH	4.36	4.98	4.16 ( <i>m</i> )
NH	6.69	8.74	8.04 ( <i>m</i> )
$\text{ArH}^{6'}$	7.89	7.92	7.68 ( <i>m</i> )
$\text{ArH}^{3'}$	8.18	8.19	7.50 ( <i>m</i> , 3H)
$\text{ArH}^8$	8.06	8.07	
$\text{ArH}^{4'}$	7.95	8.06	
$\text{ArH}^{5'}$	7.85	7.89	7.58 ( <i>m</i> , 2H)
$\text{ArH}^7$	8.13	8.09	
$\text{ArH}^6$	8.25	8.22	7.75 ( <i>m</i> )
$\text{ArH}^5$	8.60	8.63	8.05 ( <i>d</i> , $J = 8.20$ Hz)
$\text{ArH}^4$	8.92	9.36	8.67 ( <i>d</i> )

( $\delta$  162.22) was also significantly shifted upfield with respect to that in **1a** ( $\delta$  168.12 and  $\delta$  168.38). A notable geometrical feature that might provide a plausible rationale for the observed chemical shifts for  $\text{C}=\text{O}$  is the distortion between the planes of the isoquinolinyl ring and the amide group, as represented by  $\phi_3$ . While the *Z* form of **1b** has essentially no distortion ( $\phi_3 = 0.3^\circ$ ), all others have a sizable distortion from planarity, i.e., *E* of **1b** ( $\phi_3 = 43.1^\circ$ ), *Z* of **1a** ( $\phi_3 = 48.5^\circ$ ), and *E* of **1a** ( $\phi_3 = 49.3^\circ$ ). This has led us to hypothesize that the planarity between the isoquinolinyl ring and the amide group gives rise to the strong shielding of the carbonyl carbon of **1b**. A plot of the calculated chemical shift for  $\text{C}=\text{O}$  as a function of the dihedral angle,  $\phi_3$ , in **1b** (Figure 7) indeed demonstrated that shielding increases as  $\phi_3$  changes from  $\pm 40^\circ$  to  $0^\circ$ . The exact nature of the strong magnetic anisotropy of the isoquinolinyl ring on the  $\text{C}=\text{O}$  of *desmethyl-Z* is being investigated. Nonetheless, this unusual shielding can be a useful prominent marker for the *Z* rotamer of **1b** in particular as well as for other benzamides.

**Dynamics of *E* and *Z* Rotamer Interconversion in **1a**.** Having successfully characterized the *E* and *Z* isomers of **1a** and **1b** in solution via experimental and calculated  $^1\text{H}/^{13}\text{C}$  chemical shifts, we also investigated isomer interconversion by utilizing dynamic NMR and quantum chemistry. At elevated temperatures, each duplicate  $^1\text{H}$  NMR signal from the amide bond rotamers of **1a** merges to give a single peak at a specific coalescence temperature,  $T_c$ .  $T_c$  values were measured on **1a** in  $d_6$ -DMSO for the well-defined signal pairs from the  $\text{N}-\text{CH}_3$ , *s*-butyl  $\text{CH}$ , *s*-butyl  $\text{CH}_2\text{CH}_3$ , and  $\text{C4H}$  protons. Free energies for the rotation barriers *Z* to *E* as well as *E* to *Z* were then calculated by the method of Shanan-Atidi and Bar-Eli.<sup>41</sup>

**Figure 7.** Calculated  $^{13}\text{C}$ -chemical shifts of the carbonyl carbon as a function of  $\phi_3$  in **1b**.

The values derived for these two barriers from each of the four pairs of  $^1\text{H}$  NMR signals are in excellent agreement (17.1 to 17.8 kcal/mol; Table 3) and are in the range that is often observed for tertiary amides.<sup>35</sup> The *E* rotamer was found to be more stable than the *Z* rotamer by about 0.38–0.48 kcal/mol at  $T_c$  values of 57–104  $^\circ\text{C}$ .

The rate ( $k_r$ ) of *E/Z* rotation may be estimated at each coalescence temperature as  $(\pi/2^{1/2})\Delta\nu$ , if the small differences in *E* and *Z* rotamer populations are neglected.<sup>42</sup> These rates are listed in Table 3 at each of the four recorded coalescence temperatures. They are comparable to rates determined for several other tertiary aryl amides.<sup>43</sup> As the rate data for amide bond rotation in **1a** were obtained at coalescence temperatures spread over 34  $^\circ\text{C}$ , it was possible to draw an Arrhenius plot of  $\ln k_r$  versus  $1/T$  (Figure S8, Supporting Information). Although, based on only 4 points, this plot was found to be highly linear ( $r^2 = 0.976$ ) and allowed the Arrhenius activation energy ( $E_a$ ) to be derived from its slope ( $-E_a/R$ ). The value obtained for  $E_a$  is 16.5 kcal/mol, which is just 1 kcal/mol lower than the mean estimate of the free energy barrier to rotation ( $\Delta G^\ddagger = 17.5$  kcal/mol) (Table 3). Since  $E_a = \Delta H^\ddagger + RT$ , the enthalpy of activation  $\Delta H^\ddagger$  may be estimated and then also the entropy of activation  $\Delta S^\ddagger$ , according to  $\Delta G^\ddagger = \Delta H^\ddagger - T\Delta S^\ddagger$ . The values obtained were  $\Delta H^\ddagger = 15.9$  kcal/mol, and  $\Delta S^\ddagger = -5.33$  cal $^\circ\text{C}^{-1}\cdot\text{mol}^{-1}$ . The small negative value for  $\Delta S^\ddagger$  is in accord with constrained vibrational motions at the transition state and is also consistent with similar values reported for other amide bond rotations.<sup>42–44</sup> Finally, the intercept of the Arrhenius plot at  $1/T = 0$  gives 12.40 as the value for the  $\log_{10}$  of the frequency factor ( $A$ ), which is also in the range reported for amide bond rotations, such as those in *N,N*-dimethylformamide.<sup>45,46</sup> The Arrhenius plot permits estimation of the rate of rotation at any temperature of interest (e.g.,  $k_r$  is estimated to be  $\sim 1$  Hz at 20  $^\circ\text{C}$ ).

Dynamic NMR in  $\text{CDCl}_3$  also showed coalescence of each of the two pairs of  $\text{N}-\text{CH}_3$  signals from which the barrier for the chlorophenyl group rotation was readily estimated (Table 4). The rate of rotation at the measured coalescence temperatures (45 and 44  $^\circ\text{C}$  for *Z* and *E* rotamers, respectively) was estimated according to the expression  $k_r = (\pi/2^{1/2})\Delta\nu$  to be of the order of 7 to 12 Hz. This estimate may be quite accurate because members of each rotamer pair have almost equal population. Scrutiny of the same  $^1\text{H}$ -NMR spectra revealed that the two singlets for the C-4 aryl hydrogen were also split into two

Table 3. Experimentally Determined Energy Barriers for Amide Bond Rotation in **1a** in  $d_6$ -DMSO<sup>a</sup>

<sup>1</sup> H NMR signal	$\delta$ (ppm)		$ \Delta\nu $ (Hz)	$\Delta P$ ( $P_E - P_Z$ )	$T_c$ (°C)	(kcal/mol)			$k_r$ (Hz)
	Z	E				$\Delta G^{\ddagger}_E$	$\Delta G^{\ddagger}_Z$	$\Delta G^{\ddagger}_{(E-Z)}$	
N-CH <sub>3</sub>	2.77	2.85	29.8	0.288	71	17.8	17.4	0.38	66
<i>s</i> -Bu CH <sub>2</sub> CH <sub>3</sub>	0.90	0.69	80.7	0.286	85	17.8	17.5	0.39	179
<i>s</i> -Bu CH	4.61	3.72	357	0.294	104	17.7	17.3	0.41	793
C4-H	8.13	8.09	16.0	0.340	57	17.6	17.1	0.48	36

<sup>a</sup>Previously undefined column headings are defined as follows:  $\Delta\nu$  = difference in chemical shifts for *E* and *Z* <sup>1</sup>H NMR signals.  $\Delta P$  = difference in fractional populations between *Z* ( $P_Z$ ) *E* ( $P_E$ ) and rotamers.  $\Delta G^{\ddagger}_Z$  = activation energy for rotation from *Z* rotamer.  $\Delta G^{\ddagger}_E$  = activation energy for rotation from *E* rotamer.  $\Delta G^{\ddagger}_{(E-Z)} = \Delta G^{\ddagger}_E - \Delta G^{\ddagger}_Z$ .  $k_r$  = rate of rotation of bond at stated coalescence temperature ( $T_c$ ).

Table 4. Experimentally Determined Energy Barriers for 2-Chlorophenyl Group Rotation in **1a** in CDCl<sub>3</sub>

<sup>1</sup> H NMR signal	$\delta$ (ppm)		$ \Delta\nu $ (Hz)	$\Delta P$ ( $P_A - P_B$ )	$T_c$ (°C)	(kcal/mol)			$k_r$ (Hz)
	signal A	signal B				$\Delta G^{\ddagger}_A$	$\Delta G^{\ddagger}_B$	$\Delta G^{\ddagger}_{(A-B)}$	
N-CH <sub>3</sub> ( <i>Z</i> )	2.90	2.89	5.28	0.100	45	17.3	17.2	0.10	12
C4-H ( <i>Z</i> )	8.04	8.07	15.5	0.077	55	17.1	17.0	0.08	35
N-CH <sub>3</sub> ( <i>E</i> )	2.98	2.98	3.00	0.270	44	18.1	17.5	0.63	7
C4-H ( <i>E</i> )	8.01	7.99	5.40	0.143	57	18.0	17.8	0.21	12

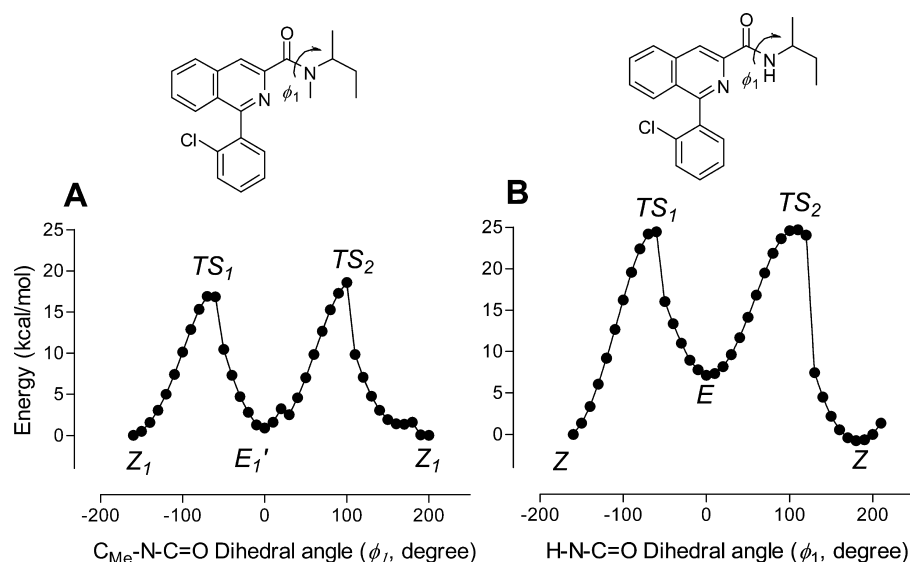


Figure 8. Potential energy versus amide group dihedral angle ( $\phi_1$ ) in **1a** (panel A) and in **1b** (panel B). Ground and transition states before full geometry optimization are indicated by their labels.

peaks of almost equal intensity. Each pair of peaks merged at coalescence temperatures of 55 and 57 °C for the *Z* and *E* rotamers, respectively (Table 4). The energy barriers for chlorophenyl group rotation (e.g.,  $\Delta G^{\ddagger}_A = 18.0$  kcal/mol) obtained from the coalescence of the C4-H peaks agree exceptionally well with those determined from the respective *N*-methyl signals (e.g.,  $\Delta G^{\ddagger}_A = 18.1$  kcal/mol). The  $\Delta G^{\ddagger}_A$  of 18.0 kcal/mol for the *E* is 1.0 and 0.4 kcal/mol higher than that for the respective chlorophenyl group rotation of the *Z* and the amide bond rotation energy barrier ( $\Delta G^{\ddagger}_E = 17.6$  kcal/mol), suggesting that the interconversion of the four isomers shown in Figure 2 occurs over a similar time scale. Rates for chlorophenyl group rotation in the *E* and *Z* isomers were also estimated (Table 4). No attempt was made to obtain Arrhenius equation parameters from these data which are for only two close  $T_c$  values.

**Potential Energy Surfaces (PESs) for the Interconversion of *Z* and *E* Rotamers of **1a** and **1b**.** In view of our <sup>1</sup>H NMR observations, revealing four quite stable rotamers of **1a**,

but not of **1b**, the PES for the conversion of both **1a** and **1b** was constructed in order to gain further insight into kinetic processes based on the structure and energetics of their ground and transition states.

We obtained the PES of **1a** in the gaseous phase at the level of B3LYP/6-31G\* by varying the  $\phi_1$  ( $C_{Me}-N-C=O$ ) from  $-164.7^\circ$  to  $175.3^\circ$  with an increment of  $10^\circ$  while relaxing the rest of the structure (Figure 8, panel A). This PES shows a steady rise in energy as the amide central C–N bond of  $Z_1$  weakens. Upon passing over the first energy barrier, another stable conformer ( $E_1'$ ) forms, which resembles *E*, but has the opposite orientation of the amide group with respect to the isoquinoline ring. Further change in  $\phi_1$  converts  $E_1'$  back to  $Z_1$  after passing the second energy barrier. Transition state (TS) geometry optimization, at the level of B3LYP/6-31G\* in the solvent reaction field of chloroform, at these two high energy points gave the two TSs with energy barriers of 18.7 and 20.1 kcal/mol at  $\phi_1 = -64.8^\circ$  and  $105.3^\circ$ , respectively. Both TSs are characterized by a weakened C–N bond (1.43 Å)

**Table 5. Energies and Geometrical Parameters of 1a and 1b Optimized at the B3LYP/6-31G\* Level in the Solvent Reaction Field of Chloroform with the PCM Model**

structure	state	$\phi_1$ ( $^\circ$ )	N–C(O) bond length (Å)	electronic energy + thermal enthalpy <sup>a</sup> (kcal/mol)	electronic energy + thermal free energy <sup>a</sup> (kcal/mol)	entropy (cal·mol <sup>-1</sup> ·K <sup>-1</sup> )
1a	Z <sub>1</sub>	-165.2	1.36	0	0	165
1a	TS <sub>1</sub>	-64.8	1.43	16.5	18.7	158
1a	TS <sub>2</sub>	105.3	1.43	18.6	20.1	160
1a	E <sub>1</sub> '	-0.7	1.36	1.2	1.3	165
1b	Z	-176.7	1.35	0	0	159
1b	TS <sub>1</sub>	-62.8	1.43	23.8	25.7	153
1b	TS <sub>2</sub>	108.2	1.43	24.0	25.4	154
1b	E	2.1	1.36	7.1	7.4	158

<sup>a</sup>Relative energetics at 298.15 K.

relative to that in the ground states (1.36 Å) and also by a single imaginary vibrational frequency (Figure S9, Supporting Information). The fully geometry-optimized conformer E<sub>1</sub>' with the  $\phi_3 = -36.0^\circ$  is 1.1 kcal/mol less stable than E<sub>1</sub> with the  $\phi_3 = 40.2^\circ$ . The calculated activation free energy ( $\Delta G^\ddagger$ ) going from E<sub>1</sub> to E<sub>1</sub>' is 4.1 kcal/mol, rendering these forms unresolvable by NMR at room temperature. The calculated  $\Delta G^\ddagger$  of 18.7 kcal/mol from Z<sub>1</sub> to E<sub>1</sub>' in 1a (Table 5) is comparable to 17.4 kcal/mol as determined with <sup>1</sup>H NMR for the coalescence of the N-CH<sub>3</sub> signal in d<sub>6</sub>-DMSO. Calculation also gave estimates of  $\Delta H^\ddagger$  (16.5 kcal/mol) and  $\Delta S^\ddagger$  ( $-7.21$  cal·K<sup>-1</sup>·mol<sup>-1</sup>) in good agreement with our experimental estimates ( $\Delta H^\ddagger = 15.9$  kcal/mol and  $\Delta S^\ddagger = -5.33$  cal·°C<sup>-1</sup>·mol<sup>-1</sup>).

The PES for the conversion of Z to E for 1b is very similar to that of 1a in that it has two minimal energy conformations that are distinguished as E and Z rotamers with H–N–C=O ( $\phi_1$ ) torsion angles of 2.1° and -176.7°, respectively (Figure 8, panel B). However, the barrier for Z to E rotation in this secondary amide is 6.7 kcal/mol greater than that in 1a due to the extra stabilization of the Z form, as discussed earlier. The greater stability of the Z rotamer is also reflected a slightly shorter amide bond length ((N–CO), 1.35 Å) than in the E rotamer (1.36 Å) (Table 5).

**PES for the Rotation of the Chlorophenyl Ring.** Figure 9 depicts the PES for varying chlorophenyl group rotation ( $\phi_4$ ) in the Z<sub>1</sub> isomer of 1a. The respective first and second energy barriers are 16.5 and 19.7 kcal/mol in the gaseous phase without zero-point and thermal contribution. Upon subjecting 1a to further TS geometry optimization in the solvent reaction field of chloroform, the  $\Delta G^\ddagger$  for the first and second TSs were calculated to be 19.8 and 24.1 kcal/mol, respectively. The larger second TS energy barrier mainly arises from the stronger steric repulsion between the Cl atom and the C8-H atom of the isoquinolinyl moiety (Figure S10, Supporting Information). When the calculation was performed on deschloro-1a (7), the barrier for the first TS was reduced to 7.8 kcal/mol. This indicates that the steric repulsion between the nonbonding sp<sup>2</sup> electrons of the isoquinoline nitrogen and the chlorine atom at the first TS in 1a amounts to about 12 kcal/mol and thus hinders the chlorophenyl group rotation significantly. A similar trend was observed for the chlorophenyl group rotation in the E<sub>1</sub> isomer, resulting in the first TS energy barrier of 18.9 kcal/mol (Table 6). Interestingly, the N-desmethyl compound 1b has a comparable energy barrier (20.0 kcal/mol), indicating that the N-methyl group does not much influence the rotational barrier of the chlorophenyl ring. The calculated values are 2.5 and 0.8 kcal/mol higher, respectively, than the experimental  $\Delta G^\ddagger$  values for the N-CH<sub>3</sub> (Z) and N-CH<sub>3</sub> (E). The discrepancy of

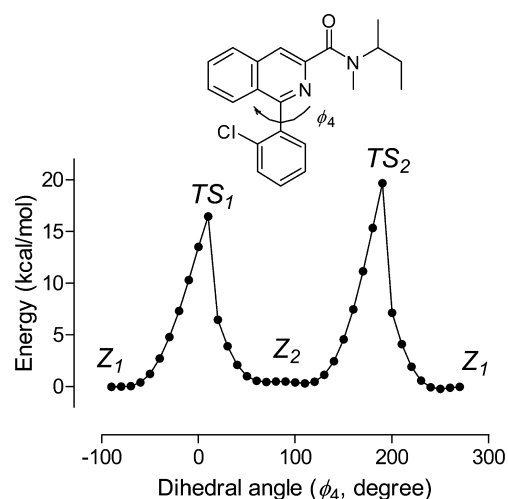


**Figure 9.** Potential energy versus chlorophenyl group rotation in the Z<sub>1</sub> isomer of 1a. Ground and transition states before full geometry optimization are indicated by their labels.

2.5 kcal/mol for the chlorophenyl group rotation of Z<sub>1</sub> might be attributed to the lack of explicit solvation in calculations or other reaction paths with a lower energy barrier that were not explored in the present study. The latter appears to be plausible because the calculated  $\Delta G^\ddagger$  was reduced to 18.6 kcal/mol when another conformer of Z<sub>1</sub>' with the  $\phi_3 = -37.1^\circ$  was employed (Table 6).

**Additional Conformers of 1a Arising from the Rotation of  $\phi_3$  and Interconversion Paths.** Besides the four stable isomers that are interconvertible via the rotation of  $\phi_1$  or  $\phi_4$  at room temperature, four additional isomers Z<sub>1</sub>', Z<sub>2</sub>', E<sub>1</sub>', and E<sub>2</sub>' (Figure 10) were obtained through the rotation of  $\phi_3$ . Interestingly, these two sets of four isomers are conformationally diastereoisomeric since the counter-clockwise rotation of  $\phi_3$  with respect to the C3–CO bond results in almost an inversion of the amide group. For example, Z<sub>1</sub>' with ( $\phi_3 = -50.3^\circ$  and  $\phi_4 = -99.9^\circ$ ) is diastereomeric to Z<sub>2</sub> ( $\phi_3 = 48.0^\circ$  and  $\phi_4 = 104.4^\circ$ ). The Z<sub>1</sub>' form was observed in the X-ray structure of 1a and is calculated to be less stable by 0.7 kcal/mol than Z<sub>1</sub> at the level of B3LYP/6-311+G(2d,p). However, the calculated  $\Delta G^\ddagger$  between Z<sub>1</sub> and Z<sub>1</sub>' is only 3.8 kcal/mol, making these rotamers unresolvable at room temperature. When such rapid interconversion occurs in solution, calculated chemical shifts with a weighted average may compare better with experimental NMR data. However, this will require an accurate energy calculation together with an explicit solvent model. Our calculated NMR chemical shifts for Z<sub>1</sub>, Z<sub>2</sub>, E<sub>1</sub>, and



**Table 6. Chlorophenyl Group Rotational Energy Barriers for 1a, Deschloro-1a (7), and 1b Obtained at the B3LYP/6-31G\* Level in the Solvent Reaction Field of Chloroform with the PCM Model**

compd	state	$\phi_4$ (°)	electronic energy + thermal enthalpy <sup>a</sup> (kcal/mol)	electronic energy + thermal free energy <sup>a</sup> (kcal/mol)	entropy (cal.mol <sup>-1</sup> .K <sup>-1</sup> )
1a	Z <sub>1</sub>	-107.6	0	0	165
1a	TS	11.5	17.0	19.8	156
1a	Z <sub>2</sub>	82.0	0.4	-0.1	167
1a	E <sub>1</sub>	-105.9	0	0	164
1a	TS	11.6	17.3	18.9	159
1a	E <sub>2</sub>	71.8	0.5	0.6	164
1a	Z <sub>1</sub> '	-106.7	0	0	163
1a	TS	-11.5	16.2	18.6	156
1a	Z <sub>2</sub> '	106.6	-0.4	-0.3	163
7	Z	-129.4	0	0	156
7	TS	5.9	6.9	7.8	153
1b	Z	-106.7	0	0	159
1b	TS	11.1	17.7	20.0	151

<sup>a</sup>Relative energetics at 298.15 K.

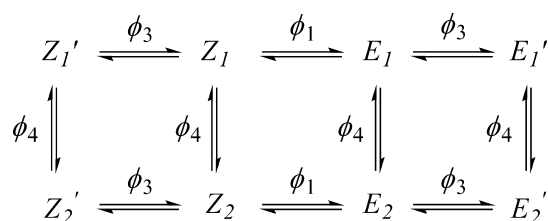


**Figure 10.** Possible interconversion pathways for 1a.

$E_2$  are, nonetheless, very compatible with experimental findings, and thus, we made no attempts to calculate the weighted NMR chemical shifts. The calculated <sup>13</sup>C chemical shifts for  $Z_1'$ ,  $Z_2'$ ,  $E_1'$ , and  $E_2'$  (Figure S11, Supporting Information) exhibit a pattern similar to those in Figure 2 and are provided for comparison.

Figure 10 also depicts a number of possible interconversion paths among the eight rotamers of 1a. For example, the conversion of  $Z_1$  to  $E_2$  may well proceed via the path of  $Z_1$ - $E_1$ - $E_2$  or  $Z_1$ - $Z_2$ - $E_2$ . A valid question is then whether this conversion would occur in a concerted or discrete manner. Dynamic NMR clearly showed two distinct coalescent processes associated with the amide bond as well as chlorophenyl group rotation. In support of the dynamic NMR finding, the calculated TS structures (Figures S9 and S10, Supporting Information) do not show a sizable steric clash between the alkyl portion and the chlorophenyl group of 1a. All these data suggest that the conversion of  $Z_1$  to  $E_2$  or vice versa occurs largely in a discrete manner.

**TSPO Preferentially Binds the E Form?** The fact that 1a exists as interconvertible rotamers that are energetically similar raises an interesting question as to which rotamer is better recognized by TSPO. One possibility is that TSPO prefers to bind amide rotamers with an *E* configuration. As is the case for 1b, the *E* configuration may be considered generally to be absent in secondary amides.<sup>35</sup> A preference for TSPO to bind *E* rotamers would be consistent with the observation that TSPO invariably binds tertiary amides much more strongly than their corresponding secondary amides, as illustrated by several

examples (Table S3, Supporting Information).<sup>25,47</sup> Thus, for the tertiary/secondary amide pair, 1a/1b, the difference in energy of binding to TSPO estimated from the  $IC_{50}$  values is about 4.4 kcal/mol. [The difference in TSPO binding energy ( $\Delta B_E$ ) for 1a and 1b may be estimated according to  $\Delta B_E = RT \cdot [\ln(^{1b}IC_{50}/^{1a}IC_{50})]$ , where  $R$  is the gas constant (1.986 cal °C/mol),  $T$  is the absolute temperature (4 °C = 277.15 K), and  $^{1a}IC_{50}$  and  $^{1b}IC_{50}$  are the  $IC_{50}$  values for the binding of 1a and 1b, respectively, to TSPO.] The approximate energy parity of the *Z* and *E* rotamers of 1a, compared to the large energy disparity (5.8 kcal/mol) between the amide bond rotamers of 1b, might easily account for this binding energy difference. Moreover, in a few known cases, where a quinoline or isoquinoline tertiary amide ligand has been constrained to the *Z* form, the affinity for TSPO is low by several thousand-fold relative to the structurally closest unconstrained tertiary amide ligand (c.f., 8 with 1c, Table S3, Supporting Information).<sup>25,27</sup> Energetically favorable freedom to rotate to the *E* form may therefore be a prerequisite for high affinity binding of ligands based on isoquinoline/quinoline amides to TSPO.

## CONCLUSIONS

The solution structures of 1a and 1b arising from the amide bond and chlorophenyl group rotation were fully characterized. While 1a exists as both *Z* and *E* rotamers in solution, 1b exists exclusively in *Z* form. Our experimental finding that the *E* isomer of 1a is more stable than the *Z* isomer in solution together with our in-depth study of their interconversion should better inform future studies aimed at acquiring a deeper understanding of TSPO–ligand interactions and new TSPO ligand discovery for drug development and molecular imaging.

## METHODS

**Materials.** Compound 1a (racemate) was purchased from Sigma-Aldrich (USA) and (*R*)-*N*-desmethyl-1a (1b) from ABX (Germany).

**Spectroscopy.** <sup>1</sup>H NMR spectra (400.13 MHz) and <sup>13</sup>C NMR (110 MHz) were recorded with an Avance spectrometer (Bruker) in the solvent indicated with tetramethylsilane (TMS) as internal standard. The values of chemical shifts are expressed in ppm downfield from the TMS signal, and coupling constants  $J$  are expressed in Hz.

**<sup>1</sup>H NMR of 1a.** The <sup>1</sup>H NMR spectrum was obtained on 1a (26.7 mg/mL) in CDCl<sub>3</sub> at 24 °C. COSY 90, NOESY, HMBC, HMQC, and NOE spectra were also obtained to assist with signal assignment.

**Dynamic <sup>1</sup>H NMR of 1a.** Coalescence temperatures ( $T_c$ ) associated with amide bond rotation in 1a were determined by raising the temperature at which <sup>1</sup>H NMR ( $d_6$ -DMSO) spectra were obtained in 5 °C increments from 20 °C until proton signals for (i) *N*-methyl, (ii) *s*-butyl CH<sub>2</sub>CH<sub>3</sub>, (iii) *s*-butyl CH, and (iv) C4-H were each found to merge. Further spectra were then acquired to determine each of the four  $T_c$  values to within less than one °C.

Coalescence temperatures ( $T_c$ ) for 2-chlorophenyl group rotation were determined by acquiring <sup>1</sup>H NMR (CDCl<sub>3</sub>) spectra in 5 °C increments from -5 °C until the paired proton signals for *N*-methyl protons and C4-H proton in each of the *E* and *Z* rotamers were seen to coalesce. Further spectra were then acquired to determine  $T_c$  to within less than 1 °C.

Energy barriers to rotations in 1a were calculated from the acquired NMR data and  $T_c$  values according to the method of Shanan-Atidi and Bar-Ali.<sup>41</sup> For more details, see Supporting Information.

**<sup>13</sup>C NMR of 1a.** The <sup>13</sup>C NMR spectrum was obtained on 1a (26.7 mg/mL) in CDCl<sub>3</sub> at 24 °C.

**<sup>1</sup>H NMR of 1b.** The <sup>1</sup>H NMR spectrum of 1b (20 mg/mL) was recorded in CDCl<sub>3</sub> at 24 °C. HETCOR (direct HC), HMBC, and H-H COSY spectra were also obtained to assist in assignment of signals. Spectra were also run in C<sub>6</sub>D<sub>6</sub> to assist with signal assignment.

**<sup>13</sup>C NMR of 1b.** The <sup>13</sup>C NMR spectrum was obtained on **1b** (26.7 mg/mL) in CDCl<sub>3</sub> at 24 °C.

**Quantum Chemistry.** The geometries of the rotamers of **1a** and **1b** were optimized with density functional theory at the B3LYP/6-311+G(2d,p) level.<sup>48</sup> The PES for the rotation of the amide bond ( $\phi_1$ ) and of the chlorophenyl group ( $\phi_4$ ) were constructed by varying a torsional angle in increments of 10° while optimizing all other geometries in the gaseous phase at the level of B3LYP/6-31G\*. The geometries of both *E* and *Z* rotamers as well as those of the *TS*s were further optimized utilizing the polarized continuum model with the UAKS parameter sets to incorporate the solvent (CHCl<sub>3</sub>) effect. Each *TS* was confirmed by the existence of a single imaginary frequency.

**Quantum Chemical Calculation of <sup>1</sup>H and <sup>13</sup>C NMR Spectra.** Shielding values (in ppm) in the solvent reaction field of chloroform at the level of B3LYP/6-311+G(2d,p) were calculated for all carbons and protons in each rotamer of **1a** and **1b** employing the gauge-independent atomic orbital method.<sup>49</sup> <sup>1</sup>H and <sup>13</sup>C chemical shifts were obtained by subtracting the shielding value of each proton and carbon from 31.8885 and 184.0456, respectively, the calculated isotropic shielding tensor for the protons and carbons in TMS.

## ■ ASSOCIATED CONTENT

### 🔍 Supporting Information

Binding assay methods and results; details of NMR and dynamic NMR of **1a** and **1b**; Arrhenius plot; and *TS* structures. This material is available free of charge via the Internet at <http://pubs.acs.org>.

## ■ AUTHOR INFORMATION

### Corresponding Author

\*Tel: 301-594-5986. Fax: 301-480-5112. E-mail: [pikev@mail.nih.gov](mailto:pikev@mail.nih.gov).

### Author Contributions

Y.-S.L. oversaw and performed quantum chemistry, interpreted data, and contributed to writing of the manuscript, especially parts concerned with quantum chemistry. F.G.S. and E.B. performed NMR spectroscopy and contributed to NMR data interpretation. V.W.P. initiated and directed the project, designed experiments, analyzed and interpreted data, wrote major parts of the paper, and composed the final draft.

### Funding

This research was supported by the Intramural Research Program of the National Institutes of Health (CIT and NIMH).

### Notes

The authors declare no competing financial interest.

## ■ ACKNOWLEDGMENTS

We are grateful to Dr. H. Umesha Shetty (NIMH) for assistance on NMR spectroscopy. The quantum chemical study utilized PC/LINUX clusters at the Center for Molecular Modeling of the NIH (<http://cit.nih.gov>).

## ■ ABBREVIATIONS

CIT, Center for Information Technology; CNS, central nervous system; DFT, density functional theory; COSY, correlated spectroscopy; DMSO, dimethyl sulfoxide; HETCOR, heteronuclear correlation spectroscopy; HMBC, heteronuclear multiple bond correlation; HMQC, heteronuclear multiple quantum coherence; NOE, nuclear Overhauser effect; NOESY, nuclear Overhauser effect spectroscopy; NIH, National Institutes of Health; NIMH, National Institute of Mental Health; NMR, nuclear magnetic resonance; PCM, polarizable continuum model; PES, potential energy surface; PET, positron emission tomography; PK 11195, 1-(2-chlorophenyl)-*N*-meth-

yl-*N*-(1-methylpropyl)-3-isoquinolinecarboxamide; rmsd, root-mean-square deviation; TMS, tetramethylsilane; *TS*, transition state; TSPO, translocator protein

## ■ REFERENCES

- (1) Le Fur, G., Vaucher, N., Perrier, M. L., Flamier, A., Benavides, J., Renault, C., Dubroeuq, M. C., Guérémy, C., and Uzan, A. (1983) Differentiation between two ligands for peripheral benzodiazepine binding sites, [<sup>3</sup>H]ROS-4864 and [<sup>3</sup>H]PK 11195, by thermodynamic studies. *Life Sci.* 33, 449–457.
- (2) Braestrup, C., and Squires, R. F. (1977) Specific benzodiazepine receptors in rat brain characterized by high-affinity (<sup>3</sup>H)diazepam binding. *Proc. Natl. Acad. Sci. U.S.A.* 74, 3805–3809.
- (3) Parola, A. L., Yamamara, H. L., and Laird, H. E. II (1993) Peripheral-type benzodiazepine receptors. *Life Sci.* 52, 1329–1342.
- (4) Krueger, K. E. (1995) Molecular and functional properties of mitochondrial benzodiazepine receptors. *Biochim. Biophys. Acta* 1241, 453–470.
- (5) Zisterer, D. M., and Williams, D. C. (1997) Peripheral-type benzodiazepine receptors. *Gen. Pharmacol.* 29, 305–314.
- (6) Krueger, K. E., and Papadopoulos, V. (1990) Peripheral-type benzodiazepine receptors mediate translocation of cholesterol from outer to inner mitochondrial membranes in adrenocortical cells. *J. Biol. Chem.* 265, 15015–15022.
- (7) Dubroeuq, M.-C., Renault, C., and Le Fur, G. (1983) Nouveaux dérivés d'arène et d'hétéroarènicarboxamides et leur utilisation comme médicaments. Eur. Pat. 0 094 271, and Fr. Pat. 82 07217.
- (8) James, M. L., Selleri, S., and Kassiou, M. (2006) Development of ligands for the peripheral benzodiazepine receptor. *Curr. Med. Chem.* 13, 1991–2001.
- (9) Scarf, A. M., Ittner, L. M., and Kassiou, M. (2009) The translocator protein (18 kDa): central nervous system disease and drug design. *J. Med. Chem.* 52, 581–592.
- (10) Capelli, A., Mohr, P. G., Gallelli, A., Giuliani, G., Anzini, M., Vomero, S., Fresta, M., Porcu, P., Maciocco, E., Concas, A., Bigio, G., and Donati, A. (2003) Structure–activity relationships in carboxamide derivatives based on the targeted delivery of radionuclides and boron atoms by means of peripheral benzodiazepine receptor ligands. *J. Med. Chem.* 46, 3568–3571.
- (11) Selleri, S., Bruni, F., Costagli, C., Costanzo, A., Guerrini, G., Ciciani, G., Costa, B., and Martini, C. (2001) 2-Arylpyrazolo[1,5-*a*]pyrimidin-3-yl acetamides. New potent and selective peripheral benzodiazepine receptor ligands. *Bioorg. Med. Chem.* 9, 2661–2671.
- (12) Kozikowski, A. P., Ma, D., Brewer, J., Sun, S., Costa, E., Romeo, E., and Guidotti, A. (1993) Chemistry, binding affinities, and behavioral properties of a new class of “antineophobic” mitochondrial DBI receptor complex (mDRC) ligands. *J. Med. Chem.* 36, 2908–2920.
- (13) Primofiore, G., Da Settimo, F., Taliani, S., Simorini, F., Patrizi, M. P., Novellino, E., Greco, G., Abignente, E., Costa, B., Chelli, B., and Martini, C. (2004) *N,N*-Dialkyl-2-phenylindol-3-ylglyoxylamides. A new class of potent and selective ligands at the peripheral benzodiazepine receptor. *J. Med. Chem.* 47, 1852–1855.
- (14) Nakazato, A., Okubo, T., Nakamura, T., Chaki, S., Tomisawa, K., Nagamine, M., Yamamoto, K., Harada, K., and Yoshida, M. (2002) Preparation of Aryloxyaniline derivatives as therapeutic agents with high affinity for the MDR receptors. US Patent 6,476,056.
- (15) Okubo, T., Yoshikawa, R., Chaki, S., Okuyama, S., and Nakazato, A. (2004) 2-Arylpyrazolo[1,5-*a*]pyrimidin-3-yl acetamides. New potent and selective peripheral benzodiazepine receptor ligands. *Bioorg. Med. Chem.* 12, 423–438.
- (16) Suzuki, K., Zhang, M.-R., Suhara, T., Nakazato, A., and Goto, M. (2004) US Patent Appl. 0138310 A1.
- (17) Lang, S. (2002) The role of peripheral benzodiazepine receptors (PBRs) in CNS pathophysiology. *Curr. Med. Chem.* 9, 1411–1415.
- (18) Galiegue, S., Tinel, N., and Casellas, P. (2003) The peripheral benzodiazepine receptor: a promising therapeutic drug target. *Curr. Med. Chem.* 10, 1563–1572.

- (19) Dollé, F., Luus, C., Reynolds, A., and Kassiou, M. (2009) Radiolabelled molecules for imaging the translocator protein (18 kDa) using positron emission tomography. *Curr. Med. Chem.* 16, 2899–2923.
- (20) Schweitzer, P. J., Fallon, B. A., Mann, J. J., and Kumar, J. S. D. (2010) PET tracers for the peripheral benzodiazepine receptor and uses thereof. *Drug Discovery Today* 15, 933–942.
- (21) Chauveau, F., Boutin, H., Van Camp, N., Dollé, F., and Tavitian, B. (2008) Nuclear imaging of neuroinflammation: a comprehensive review of [<sup>11</sup>C]PK11195 challengers. *Eur. J. Nucl. Med. Mol. Imaging* 35, 2304–2319.
- (22) Banati, R. B. (2002) Visualising microglial activation in vivo. *Glia* 40, 206–217.
- (23) Cagnin, A., Gerhard, A., and Banati, R. B. (2002) In vivo imaging of neuroinflammation. *Eur. Neuropsychopharmacol.* 12, 581–586.
- (24) Georges, G., Vercauteren, D. P., Vanderveken, D. J., Horion, R., Evrard, G., Fripiat, J. G., Andre, J.-M., and Durant, F. (1990) Structural and electronic analysis of peripheral benzodiazepine ligands: description of the pharmacophoric elements for their receptors. *Int. J. Quant. Chem.* 17, 1–25.
- (25) Cappelli, A., Anzini, A., Vomero, S., De Benedetti, P. G., Menziani, M. C., Giorgi, G., and Manzoni, C. (1997) Mapping the peripheral benzodiazepine receptor binding site by conformationally restrained derivatives of 1-(2-chlorophenyl)-N-methyl-N-(1-methylpropyl)-3-isoquinolinecarboxamide (PK 11195). *J. Med. Chem.* 40, 2910–2921.
- (26) Cinone, N., Höltje, H.-D., and Carotti, A. (2000) Development of a unique 3D interaction model of endogenous and synthetic benzodiazepine receptor ligands. *J. Comput.-Aided Mol. Des.* 14, 753–768.
- (27) Anzini, M., Cappelli, A., Vomero, S., Seeber, M., Menziani, M. C., Langer, T., Hagen, B., Manzoni, C., and Bourguignon, J.-J. (2001) Mapping and fitting the peripheral benzodiazepine receptor binding site by carboxamide derivatives. Comparison of different approaches to quantitative ligand-receptor interaction modeling. *J. Med. Chem.* 44, 1134–1150.
- (28) Narasimhan, P. T., and Rogers, M. T. (1959) Nuclear magnetic shielding of protons in amides and the magnetic anisotropy of the C=O bond. *J. Phys. Chem.* 63, 1388–1394.
- (29) Kubicki, M., and Coddling, P. W. (2001) 1-(2-Chlorophenyl)-N-methyl-N-(1-methylpropyl)-isoquinoline carboxamide. *Acta Crystallogr., Sect. E* 57, o-389–o391.
- (30) Kaupp, M., Bühl, M., and Malkin, V. G., Eds. (2004) *Calculation of NMR and EPR Parameters*, Wiley-VCH, Weinheim, Germany.
- (31) Jiao, D., Barfield, M., and Hruba, V. J. (1993) *Ab initio* IGLO study of the *syn/anti* dependence of the <sup>13</sup>C NMR chemical shifts in simple amides. *Magn. Reson. Chem.* 31, 75–79.
- (32) Dorie, J., Gouesnard, J. P., Mechin, B., Maulet, N., and Martin, G. J. (1980) Applications of <sup>15</sup>N-NMR spectroscopy to the study of unsymmetrically substituted amides and model peptide compounds. *Org. Mag. Res.* 13, 126–131.
- (33) Raynes, W. T., and Sutherley, T. A. (1970) Origin of the chemical shift due to hindered rotation in N,N-dimethylformamide. *Mol. Phys.* 18, 129–131.
- (34) McFarlane, W. (1970) Heteronuclear magnetic double resonance measurement of carbon-13 chemical shifts in NN-dimethylformamide and related compounds. *Chem. Commun.*, 418–419.
- (35) Stewart, W. E., and Siddall, T. H. III (1970) Nuclear magnetic resonance studies of amides. *Chem. Rev.* 5, 517–551.
- (36) Paulsen, H., and Todt, K. (1966) Magnetic anisotropy of the amide group. *Angew. Chem., Int. Ed.* 5, 899–900.
- (37) La Planche, L. A., and Rogers, M. T. (1964) *cis* and *trans* Configurations of the peptide bond in N-monosubstituted amides by nuclear magnetic resonance. *J. Am. Chem. Soc.* 86, 337–341.
- (38) Nagarajan, K., Nair, M. D., and Pillai, P. M. (1967) Configuration of the amide bond in N-acylindolines and N-acyltetrahydroquinolines. *Tetrahedron* 23, 1683–1690.
- (39) Lewin, A. H., and Frucht, M. (1975) Restricted rotation in amides. VII—Methods of resonance assignment in tertiary amides—An evaluation. *Org. Mag. Res.* 7, 206–225.
- (40) Hassan, S. A. (2007) Liquid-structure forces and electrostatic modulation of biomolecular interactions in solution. *J. Phys. Chem. B* 111, 227–241.
- (41) Shanan-Atidi, H., and Bar-Eli, K. H. (1970) A convenient method for obtaining free energies of activation by the coalescence temperature of an unequal doublet. *J. Phys. Chem.* 74, 961–963.
- (42) Piccinni-Leopardi, C., Fabre, O., and Reisse, J. (1976) Determination of  $\Delta H^\ddagger$  and  $\Delta S^\ddagger$  by simultaneous <sup>1</sup>H and <sup>13</sup>C-dynamic n.m.r. studies: importance of the accuracy of temperature measurement. *Org. Mag. Res.* 8, 233–236.
- (43) Pinto, B. M., Grindley, T. B., and Szarek, W. A. (1986) Effects of substitution on nitrogen barriers to rotation of amides. *Magn. Reson. Chem.* 24, 323–331.
- (44) Rabinovitz, M., and Pines, A. (1969) Hindered internal rotation and dimerization of N,N-dimethylformamide in carbon tetrachloride. *J. Am. Chem. Soc.* 91, 1585.
- (45) Sandström, J. (1982) Evaluation of Activation Parameters, in *Dynamic NMR Spectroscopy*, Chapter 7, pp 93–123. Academic Press, New York.
- (46) Kessler, V. H. (1970) Nachweis gehinderter Rotationen und Inversionen durch NMR-Spektroskopie. *Angew. Chem.* 82, 237–253.
- (47) Bourguignon, J. J. (1993) Endogenous and Synthetic Ligands of Mitochondrial Benzodiazepine Receptors: Structure–Affinity Relationships, in *Peripheral Benzodiazepine Receptors*. (Giesen-Crouse, E., Ed.) Ch. 3, pp 59–85, Academic Press, London.
- (48) Frisch, M. J., Trucks, G. W., Schlegel, H. B., Scuseria, G. E., Robb, M. A., Cheeseman, J. R., Scalmani, G., Barone, V., Mennucci, B., Petersson, G. A., Nakatsuji, H., Caricato, M., Li, X., Hratchian, H. P., Izmaylov, A. F., Bloino, J., Zheng, G., Sonnenberg, J. L., Hada, M., Ehara, M., Toyota, K., Fukuda, R., Hasegawa, J., Ishida, M., Nakajima, T., Honda, Y., Kitao, O., Nakai, H., Vreven, T., Montgomery, J. A. Jr., Peralta, J. E., Ogliaro, F., Bearpark, M., Heyd, J. J., Brothers, E., Kudin, K. N., Staroverov, V. N., Kobayashi, R., Normand, J., Raghavachari, K., Rendell, A., Burant, J. C., Iyengar, S. S., Tomasi, J., Cossi, M., Rega, N., Millam, J. M., Klene, M., Knox, J. E., Cross, J. B., Bakken, V., Adamo, C., Jaramillo, J., Gomperts, R., Stratmann, R. E., Yazyev, O., Austin, A. J., Cammi, R., Pomelli, C., Ochterski, J. W., Martin, R. L., Morokuma, K., Zakrzewski, V. G., Voth, G. A., Salvador, P., Dannenberg, J. J., Dapprich, S., Daniels, A. D., Farkas, Ö., Foresman, J. B., Ortiz, J. V., Cioslowski, J., Fox, D. J. (2009) *Gaussian 09*, revision A.02, Gaussian, Inc., Wallingford CT.
- (49) Cheesman, J. R., Trucks, G. W., Keith, T. A., and Frisch, M. J. (1996) A comparison of models for calculating nuclear magnetic resonance shielding tensors. *J. Chem. Phys.* 104, 5497–5509.